

# Magnetization steps and cluster-type statistics for a diluted Heisenberg antiferromagnet on the square lattice: Models with two exchange constants

Yaacov Shapira\*

*Department of Physics and Astronomy, Tufts University, Medford, MA 02155*

Valdir Bindilatti†

*Instituto de Física, Universidade de São Paulo,  
Caixa Postal 66.318, 05315-970 São Paulo-SP, Brazil*

(Dated: May 1, 2019)

Magnetization steps (MST's) from a strongly diluted antiferromagnet on the square lattice are discussed theoretically. Thermal equilibrium, at temperature  $T$  and magnetic field  $B$ , is assumed. Two specific cluster models with the largest and second-largest exchange constants,  $J^{(1)}$  and  $J^{(2)}$ , respectively, are considered in detail. In the  $J_1$ - $J_2$  model,  $J^{(1)}$  is the nearest-neighbor (NN) exchange constant  $J_1$ , and  $J^{(2)}$  is the second-neighbor exchange constant  $J_2$ . In the  $J_1$ - $J_3$  model,  $J^{(1)}=J_1$ , and  $J^{(2)}$  is the third-neighbor exchange constant  $J_3$ . For these two models, all cluster types of sizes  $n_c \leq 5$  are identified, and their statistics is expressed using perimeter polynomials for cluster types. All cluster types with sizes  $n_c > 1$  give rise to MST's. Calculated curves of the isothermal magnetization  $M$  as a function of  $B$  are given for widely different ratios  $J^{(2)}/J^{(1)}$ . Some of the information contained in these magnetization curves is conveyed more directly by the derivative curves,  $dM/dB$  versus  $B$ . The series of peaks in the derivative curve is called the "MST spectrum." This spectrum is much simpler when the ratio  $J^{(2)}/J^{(1)}$  is very small. A detailed discussion of the exchange-bond structure and MST spectra for cluster models with a very small ratio  $J^{(2)}/J^{(1)}$  is given in the following paper. The "parent" models of the  $J_1$ - $J_2$  model are the  $J_1$  and  $J_2$  models. For the  $J_1$ - $J_3$  model the parent models are the  $J_1$  and  $J_3$  models. Relations between the  $J_1$ - $J_2$  and the  $J_1$ - $J_3$  models and their respective parent models are discussed. The three parent cluster models ( $J_1$ -,  $J_2$ -, and  $J_3$ -models) are identical, except for the neighbor associated with the one exchange constant  $J$  that is included in the model. Common properties of such "isomorphic" cluster models are discussed.

PACS numbers: 05.50.+q, 75.50.Ee, 71.70.Gm, 75.10.Jm, 75.10.Nr, 75.60.Ej

## I. INTRODUCTION

An earlier theoretical paper<sup>1</sup> (hereafter I) on magnetization steps from a diluted Heisenberg antiferromagnet on the square lattice was largely devoted to the nearest-neighbor (NN) cluster model. To obtain magnetization steps (MST's), the NN exchange constant  $J_1$  must be antiferromagnetic (AF). The present paper discusses cluster models with two exchange constants: the largest, called  $J^{(1)}$ , and the second-largest,  $J^{(2)}$ . Both exchange constants are assumed to be AF.

Some of the discussion in the present paper applies to any  $J^{(1)}$ - $J^{(2)}$  cluster model, regardless of the neighbors associated with  $J^{(1)}$  and  $J^{(2)}$ . However, the main focus is on the  $J_1$ - $J_2$  and  $J_1$ - $J_3$  models. In these models  $J^{(1)}=J_1$ , and  $J^{(2)}$  is either the second-neighbor exchange constant  $J_2$ , or the third-neighbor exchange constant  $J_3$ .

As in I, the following assumptions are made: 1) Thermal equilibrium, at temperature  $T$  and magnetic field  $B$ , prevails. 2) All the magnetic ions are identical. 3) The cation sites form a square lattice, and the magnetic ions are randomly distributed over these sites. 4) Only a fraction  $x$  of all cations sites are occupied by magnetic ions. This fraction is well below the site percolation concentration  $x_c$  for the relevant cluster model. 5) None of the magnetic interactions is anisotropic. Background mate-

rial for the present paper may be found in I, in a recent review,<sup>2</sup> and in earlier papers.<sup>3,4,5</sup>

This paper is organized as follows. The principal results are presented in the main text. Supplementary material is relegated to appendices. The main text starts with a brief discussion of the crucial role of cluster "configurations" in the theory. All cluster types in the  $J_1$ - $J_2$  and  $J_1$ - $J_3$  models, subject to the restriction  $n_c \leq 5$  on the cluster size  $n_c$ , are then identified. The statistics for these cluster types is expressed using perimeter polynomials (PP's) for cluster types. As discussed in I, the PP's for cluster types are analogous to the conventional PP's for cluster sizes.<sup>6</sup>

The contribution of any cluster type to the magnetization  $M$  is calculated by combining the results for the energy eigenvalues with those for the cluster statistics of that cluster type. The total magnetization  $M(T, B)$  is the sum of the contributions from all cluster types. In some respects the derivative curve,  $dM/dB$  versus  $B$ , is more informative than the magnetization curve,  $M$  versus  $B$ . Examples of calculated magnetization and derivative curves at constant  $T$  are given for widely different ratios  $J^{(2)}/J^{(1)}$ .

The statistics for cluster types is independent of the spin  $S$  of the individual magnetic ions. However, the energy eigenvalues, and therefore the magnetization curve, depend on  $S$ . Although much of the discussion is for any

$S$ , all the numerical examples are for  $S=5/2$ , which is the appropriate value for the  $\text{Mn}^{2+}$  and  $\text{Fe}^{3+}$  ions. Both these ions are  $S$ -state ions, and they usually have low crystalline anisotropy. Such ions are useful for testing theories in which anisotropy is neglected.

The structures of the magnetization and derivative curves are much simpler when the ratio  $J^{(2)}/J^{(1)}$  is “very small.” Cluster models with such widely different magnitudes of  $J^{(2)}$  and  $J^{(1)}$  are called “lopsided cluster models.” In addition to their interesting physics, lopsided models are useful because they apply to many materials. Lopsided cluster models are discussed in detail in the following paper.<sup>7</sup>

## II. CLUSTER CONFIGURATIONS

### A. Configurations

The calculation of the magnetization  $M(T, B)$  in any cluster model requires: 1) the identification of all cluster types  $c$  in that model; 2) a calculation of the average magnetic moment  $\mu_c(T, B)$  per realization,<sup>8</sup> for each cluster type  $c$ ; and 3) an evaluation of the probabilities of finding the various cluster types.

Before carrying out the first and third of these tasks it is necessary to identify all the “cluster configurations” that exist in the particular cluster model. These cluster configurations are the fundamental building blocks of the theory, and also of the computer programs that are used to implement the theory. Cluster configurations were discussed in Sec. IIIB of I. The discussion below brings out some new features.

#### 1. Cluster configurations

A spin cluster consists of a finite number of exchange-coupled magnetic ions (spins) that occupy a set of cation sites. Spin clusters are considered to have the same configuration if and only if the sets of cation sites occupied by these clusters can be obtained from each other by symmetry operations of the space group of the cation structure. Each one such set of cation sites is called a “realization” of the configuration.

The symmetry operations of the space group of the cation structure are the only symmetry operations considered in the present work. They will be referred to, simply, as “symmetry operations.” The symmetry operations that are relevant to the present work are the operations of the  $P4m$  space group of the square lattice, including the lattice translations.

Realizations of the same configuration have the following important geometrical property. Starting from one realization, a rigid object can be constructed by joining all pairs of cation sites in that realization by straight-line segments. The straight-line segments may be viewed as “struts” that give the object its rigidity. Rigid objects

constructed in this manner from different realizations of the same configuration, either have identical shapes or are chiral isomers (mirror images) of each other. Because of this geometrical property, configurations of clusters are sometimes viewed as the geometrical shapes of clusters.

#### 2. Cluster configurations of one specific cluster model

A cluster model is specified by the set of exchange constants (the  $J$ 's) that are included in the model. Any spin cluster in this model consists of spins that are coupled to each other, but not to other spins, by the  $J$ 's of the model. Thus, any two spins in a cluster are connected by at least one continuous path of exchange bonds associated with this set of  $J$ 's. No continuous path of such exchange bonds is allowed to exist between spins in different clusters.

The restriction on the allowed  $J$ 's is a restriction on the allowed sets of cation sites associated with the clusters of the model. For example, in the  $J_1$ - $J_2$  model, any cation site of a cluster must have a NN site or a 2nd-neighbor site in the same cluster. The cluster configurations of the model are all the configurations of the sets of cation sites that are allowed by the  $J$ 's of the model.

#### 3. Identical configurations in different cluster models

Sometimes, several cluster models are considered. It may then happen that the set of  $J$ 's in one cluster model is only a subset of all the exchange constants in another cluster model. Any cluster configuration in the cluster model with the fewer  $J$ 's is then also a configuration in the model with the larger set of  $J$ 's. For example, the exchange constant  $J_1$  of the NN cluster model is a subset of the exchange constants in the  $J_1$ - $J_2$  model. Any cluster configuration in the  $J_1$  model is also a configuration in the  $J_1$ - $J_2$  model. The converse is not true; many cluster configurations that exist in the  $J_1$ - $J_2$  model do not exist in the  $J_1$  model.

For the same reason, all cluster configurations that exist in the  $J_1$  model also exist in the  $J_1$ - $J_3$  model. Figure 2 of I shows an example of the same configuration in different cluster models. Figure 2(b) of I shows the configuration in the  $J_1$  model, and Figs. 2(c) and 2(d) show the same configuration in the  $J_1$ - $J_2$  and  $J_1$ - $J_3$  models, respectively.

### B. From cluster configurations to cluster types

Once a cluster model is specified, it is necessary to identify the cluster types that exist in the model. In the present work this identification was carried out by a series of computer program. The first set of programs identified all the (different) configurations that exist in

the specified cluster model. For each configuration, a realization that has one spin at the origin was generated. This realization is called the “prototype” of the configuration. Only configurations with no more than 5 cation sites were considered explicitly in the present work.

A cluster type  $c$  is specified by a cluster size  $n_c$  and by a bond list.<sup>1</sup> To identify the cluster types that exist in the model, the prototypes of all the (different) configurations were first classified by size, i.e., by the number of spins in the prototype. The next step was to generate the bond lists for all prototypes of a given size,  $n_c$ . The final step was to identify all prototypes of the same size  $n_c$  that have identical bond lists. Such prototypes are, by definition,<sup>8</sup> realizations of the same cluster type,  $c$ . In fact, they are the prototypes of all the configurations  $r_c$  of cluster type  $c$ .

To summarize, the classification of the prototypes of different configurations by both size and bond list leads to: 1) all cluster types  $c$ , for each cluster size  $n_c$ ; 2) the bond list for each of these cluster types; and 3) the prototypes of all the configurations of each cluster type.

### C. Statistics of cluster types

The goal of the statistics is to find, for each cluster type  $c$ , the probability  $P_c$  that a randomly-chosen spin is in one of the realizations of this cluster type. The main assumption is that the magnetic ions are randomly distributed over the cation sites. The procedure for calculating  $P_c$  as a function of  $x$  was outlined in Sec. III C of I. The procedure starts from the configurations  $r_c$  of cluster type  $c$ .

Any realization of cluster type  $c$  must also be a realization of one of the configurations  $r_c$  of that cluster type. The probability  $P_{r_c}$  that a randomly-chosen spin is in some realization of the configuration  $r_c$  is given by Eq. (4) of I. This equation contains two parameters that depend on the configuration: the lattice-combinatorial parameter  $n_{r_c}$ , and the perimeter  $\nu_{r_c}$ . After these two parameters are evaluated for each of the configurations  $r_c$ , the probability  $P_c$  is obtained by summing  $P_{r_c}$  over all the configurations  $r_c$  of cluster type  $c$ . This sum is given by Eq. (5) of I.

The lattice-combinatorial parameter  $n_{r_c}$  is the number of (distinct) realizations of the configuration  $r_c$  that have one spin at the origin. This  $n_{r_c}$  depends only on the configuration. If the same configuration exists in more than one cluster model, then the corresponding lattice-combinatorial parameters are the same in all these models. The computer program that was used to obtain  $n_{r_c}$  was based on the principle that all realizations of a configuration can be generated from the prototype of the configuration by applying the symmetry operations of the  $P4m$  space group, including the lattice translations. If the same realization was generated by different symmetry operations, the count for  $n_{r_c}$  included this realization only once.

In contrast to  $n_{r_c}$ , the perimeter  $\nu_{r_c}$  depends not only on the configuration but also on the cluster model. If the same configuration exists in two cluster models, the perimeters in the two models are, in general, not equal. For example, any configuration that is present in the  $J_1$  model is also present in the  $J_1$ - $J_2$  model. The perimeter in the  $J_1$  model will be called the  $J_1$  perimeter. Given any realization of the configuration  $r_c$ , the  $J_1$  perimeter is the number of (cation) sites that are NN’s of the sites in the realization, but are not themselves sites of the realization. The perimeter in the  $J_1$ - $J_2$  model (called the  $J_1$ - $J_2$  perimeter) is the number of sites that are either NN’s and/or 2nd-neighbors of the sites in the realization, but are not themselves sites of the realization. Therefore, for the same configuration, the  $J_1$ - $J_2$  perimeter is larger than the  $J_1$  perimeter. As a consequence, the probability that a randomly-chosen spin is in a realization of this configuration will be lower in the  $J_1$ - $J_2$  model than in the  $J_1$  model [See Eq. (4) of I]. Similar results apply to a configuration that exists in both the  $J_1$  and the  $J_1$ - $J_3$  models.

## III. CLUSTER TYPES

### A. Generic and specific models

A  $J^{(1)}$ - $J^{(2)}$  cluster model in which the symmetry classes of the neighbors associated with  $J^{(1)}$  and  $J^{(2)}$  are not specified will be called a “generic” model. If the symmetry classes of the neighbors are specified, the cluster model is “specific” rather than generic. In this paper, only two specific  $J^{(1)}$ - $J^{(2)}$  models are considered: the  $J_1$ - $J_2$  model (with  $|J_1| > |J_2|$ ), and the  $J_1$ - $J_3$  model (with  $|J_1| > |J_3|$ ). The reason for focusing on these specific models is that exchange constants often tend to decrease as the distance  $r$  of the relevant neighbor increases. Although the decrease is not always monotonic,<sup>4,5</sup> we expect that in the vast majority of diluted antiferromagnets with a square cation lattice,  $J^{(1)} = J_1$  and  $J^{(2)}$  is either  $J_2$  or  $J_3$ .

The cluster types in the  $J_1$ - $J_2$  model are not trivially related to the cluster types in the  $J_1$ - $J_3$  model. That is, the bond lists for the two models cannot be obtained from each other by replacing the  $J_2$  bonds by  $J_3$  bonds. The site percolation concentrations for these two specific models are also different.<sup>9</sup> The non-trivial dependence of the bond lists, and hence of the cluster types, on the specific cluster model implies that bond lists and cluster types cannot be given for a generic model. They can only be given for a specific model.

### B. Parent cluster models

The “parent” cluster models of the  $J_1$ - $J_2$  model are the  $J_1$  model and the  $J_2$  model, each of which has only one of exchange constants of the  $J_1$ - $J_2$  model. The  $J_1$ - $J_2$

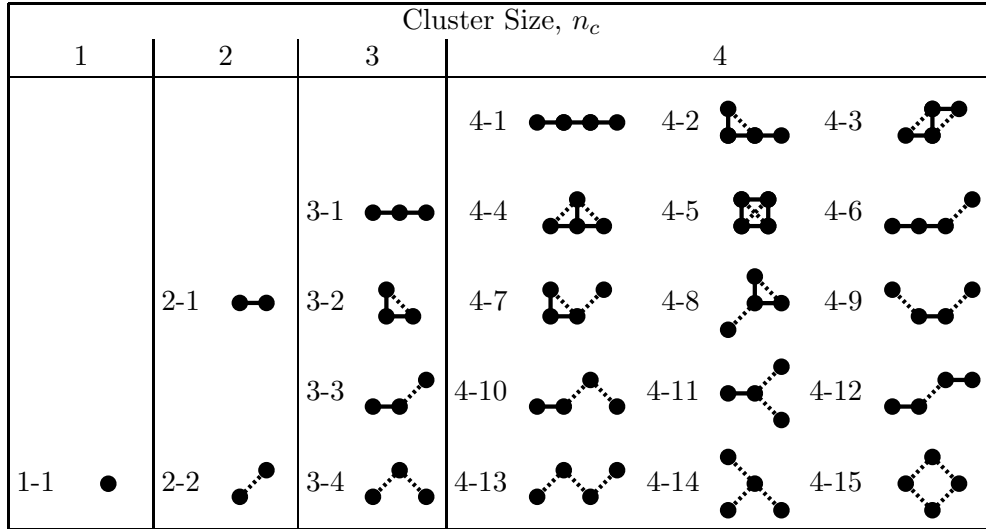


FIG. 1: Cluster types of the  $J_1$ - $J_2$  model, up to cluster size  $n_c=4$ . Solid circles represent spins. Solid and dotted lines represent  $J_1$  bonds and  $J_2$  bonds, respectively. The labels for the cluster types are discussed in the text.

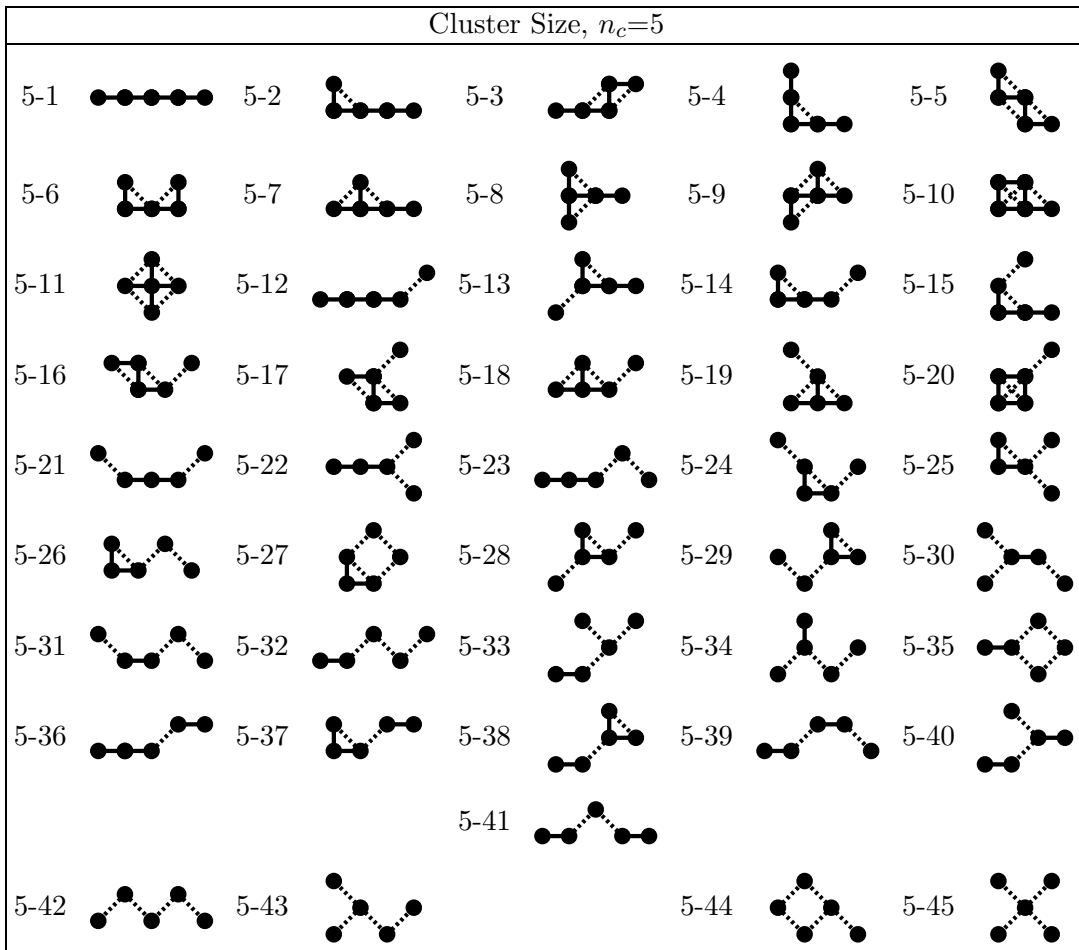


FIG. 2: Cluster types of quintets ( $n_c=5$ ) in the  $J_1$ - $J_2$  model.

model is not a simple combination of its parent models. Similarly, the  $J_1$ - $J_3$  model is not a simple combination of the  $J_1$  and  $J_3$  models, which are its parent models.

There are many interesting relations between the  $J_1$ - $J_2$  and  $J_1$ - $J_3$  models and their respective parent models. To avoid repeated interruptions in the main text of the paper, discussions of these relations are relegated to Appendices. For the limited purpose of calculating magnetization curves numerically, the results in these Appendices are not essential. However, these results give a deeper insight into the physics. Some of these results will be quoted, and used, in the main texts of the present paper and of the following paper. Appendix A, describes the strong similarity (called “isomorphism”) between the three parent models, i.e., the  $J_1$ ,  $J_2$ , and  $J_3$  models. These are the only “parent models” considered in the present work.

### C. Cluster types in the $J_1$ - $J_2$ model

#### 1. Cluster types

In the  $J_1$ - $J_2$  model on the square lattice, there are 67 cluster types of sizes  $n_c \leq 5$ . These cluster types are shown in Figs. 1 and 2. Cluster types of the same size,  $n_c$ , appear in the same column. The four columns in Fig. 1 show the cluster types with  $n_c=1, 2, 3$ , and 4. The single column in Fig. 2 shows the cluster types with  $n_c=5$ . Spins are represented by solid circles,  $J_1$  bonds by solid lines, and  $J_2$  bonds by dotted lines. Only one configuration for each cluster type is shown. The bond lists for these cluster types, which specify all intra-cluster exchange interactions,<sup>1</sup> are given in Appendix B.

Each cluster type is labeled by two numbers separated by a hyphen. The first number is the cluster size  $n_c$ . The second is a serial number (SN) within this cluster size. Thus, the format for any label is  $[n_c$ -(SN)]. There is only one type of single (type 1-1), but two types of pairs: 2-1 which is a  $J_1$ -pair, and 2-2 which is a  $J_2$ -pair. There are four types of triplets ( $n_c=3$ ), 15 types of quartets ( $n_c=4$ ), and 45 types of quintets ( $n_c=5$ ).

#### 2. Four categories of cluster types

The number of cluster types in Figs. 1 and 2 is rather large. It is therefore useful to classify them. The classification scheme is not unique. In one scheme the 67 cluster types in Figs. 1 and 2 are divided into four broad categories:

1. “single,” which has no exchange bonds;
2. “pure  $J_1$ ” cluster types, with only  $J_1$  exchange bonds;
3. “pure  $J_2$ ” cluster types, with only  $J_2$  bonds;
4. “mixed” cluster types, with both  $J_1$  and  $J_2$  bonds.

The single (type 1-1) is at the left of the bottom row of Fig. 1. The only pure  $J_2$  cluster types are the other 5 cluster types in the same bottom row together with the four cluster types in the bottom row of Fig. 2. The only pure  $J_1$  cluster types are: 2-1, 3-1, 4-1, and 5-1. All the remaining 53 cluster types are “mixed” types.

The pure  $J_1$  cluster types, and the pure  $J_2$  cluster types, are related to cluster types in the (parent)  $J_1$  and  $J_2$  models, respectively. These relations are discussed in Appendix C.

### D. Cluster types in the $J_1$ - $J_3$ model

In the  $J_1$ - $J_3$  model there are 82 cluster types of sizes  $n_c \leq 5$ . They are shown in Figs. 3 and 4. The format is the same as in Figs. 1 and 2, except that the dotted lines now represent  $J_3$  bonds. The bond lists for the cluster types in Figs. 3 and 4 are given in Appendix B.

The labels for the cluster types of the  $J_1$ - $J_3$  model have the same format as those for the cluster types in the  $J_1$ - $J_2$  model. Therefore, many of the labels used in the two models are identical. When the same label appears in both models, it often refers to different cluster types (i.e., different bond lists). Unless it is clear from the context, it is then necessary to specify the cluster model to which the label refers.

Once again the cluster types in Figs. 3 and 4 can be divided into four categories:

1. the “single” (type 1-1), at the left of the bottom row of Fig. 3;
2. the 9 “pure  $J_3$ ” cluster types, consisting of the other 5 cluster types in the bottom row of Fig. 3 together with the 4 cluster types in the bottom row of Fig. 4;
3. the 5 “pure  $J_1$ ” cluster types: 2-1, 3-2, 4-3, 4-5, and 5-5;
4. the 67 remaining cluster types, which are all “mixed” types.

## IV. CLUSTER STATISTICS AND PERIMETER POLYNOMIALS

### A. Results for small clusters

The probabilities  $P_c$  as a function of  $x$  were obtained using the procedure discussed in Sec. II C. Only cluster types with  $n_c \leq 5$  were considered. Some of the results for the  $J_1$ - $J_2$  model are shown Fig. 5. They include the  $P_c$ 's for the single (type 1-1), for the two types of pairs (2-1 and 2-2), and for the four types of triplets (3-1, 3-2, 3-3 and 3-4). These labels for the cluster types refer to Fig. 1. Also shown in Fig. 5 are: the sum  $P_4$  of the probabilities for all 15 quartet types in Fig. 1; the sum  $P_5$  of the probabilities for all the quintet types in Fig. 2;

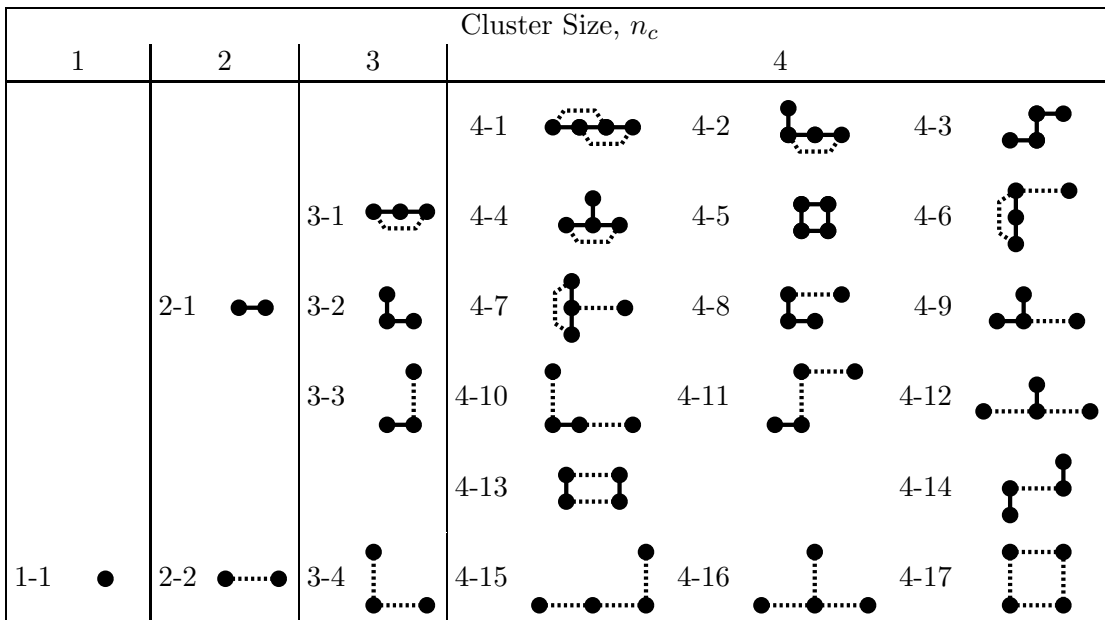


FIG. 3: Cluster types of the  $J_1$ - $J_3$  model, up to cluster size  $n_c=4$ . The format, including the format of the labels for the cluster types, is similar to that in Fig. 1, except that the dotted lines represent  $J_3$  bonds.

and the sum  $P_{>5}$  of the probabilities for all cluster types with sizes  $n_c > 5$ .

Figure 6 shows the corresponding probabilities for the  $J_1$ - $J_3$  model. In this case the cluster types refer to Figs. 3 and 4. In both Fig. 5 and Fig. 6 the highest value of  $x$  is below the relevant site percolation concentration,  $x_c=0.407$  for the  $J_1$ - $J_2$  model, and  $x_c=0.337$  for the  $J_1$ - $J_3$  model.<sup>9,10</sup> For the  $J_1$  model,  $x_c=0.593$ .

## B. Perimeter polynomials

As discussed in I, the probability  $P_c$  can be expressed succinctly in the form

$$P_c = n_c x^{n_c-1} D_c(q), \quad (1)$$

where  $D_c(q)$  is a polynomial in  $q=1-x$ , defined as the perimeter polynomial (PP) for cluster type  $c$ . Appendix B gives the PP's for cluster types with sizes  $n_c \leq 5$  in the  $J_1$ - $J_2$  model. These are the cluster types in Figs. 1 and 2. Appendix B also gives the PP's for cluster types of the  $J_1$ - $J_3$  model whose sizes are  $n_c \leq 5$ . These are the cluster types in Figs. 3 and 4.

For the  $J_1$ - $J_2$  model, the following check on the results for  $D_c(q)$  in Appendix B was performed. The conventional PP's,  $D(q)$ , for cluster sizes (not types) were given for this model by Peters et al.<sup>10</sup> As expected, the polynomial  $D(q)$  for any cluster size  $s$  is equal to the sum  $\sum D_c(q)$  of the PP's in Appendix B over all cluster types  $c$  that have the size  $n_c=s$ .

Appendix D discusses some relations between the probabilities  $P_c$  for the pure- $J_1$  and pure- $J_2$  cluster types in

the  $J_1$ - $J_2$  model and the probabilities for the same cluster types in the (parent)  $J_1$  and  $J_2$  models. The relations between the probabilities  $P_c$  for pure- $J_1$  and pure- $J_3$  cluster types in the  $J_1$ - $J_3$  model and the probabilities for the same cluster types in the (parent)  $J_1$  and  $J_3$  models are also discussed.

## V. THE MAGNETIZATION CURVE

### A. Calculation procedure

The procedure for calculating the magnetization  $M(T, B)$  was discussed previously.<sup>1,2</sup> Briefly, the Hamiltonian of one realization<sup>8</sup> of each cluster type  $c$  is diagonalized, and the results are used to obtain the average magnetic moment  $\mu_c(T, B)$  per realization. For singles,  $\mu_c(T, B)$  follows the Brillouin function for spin  $S$ . For each of the other cluster types,  $\mu_c(T, B)$  exhibits a series of MST's as a function of  $B$  at very low  $T$ .

The total magnetization  $M(T, B)$  is a statistically-weighted sum of  $\mu_c(T, B)$ . This sum is given by Eq. (13) of I, namely,

$$M(T, B) = \sum_c N_c \mu_c(T, B) = N_{\text{total}} \sum_c \frac{P_c}{n_c} \mu_c(T, B), \quad (2)$$

where  $N_c = P_c N_{\text{total}} / n_c$  is the population of cluster type  $c$ , and  $N_{\text{total}}$  is the total number of spins. The quantities  $M$ ,  $N_c$  and  $N_{\text{total}}$  are all either per unit mass or per unit volume.

The infinite sum in Eq. (2) cannot be evaluated exactly because  $\mu_c(T, B)$  and  $P_c$  (or  $N_c$ ) are known only for a fi-

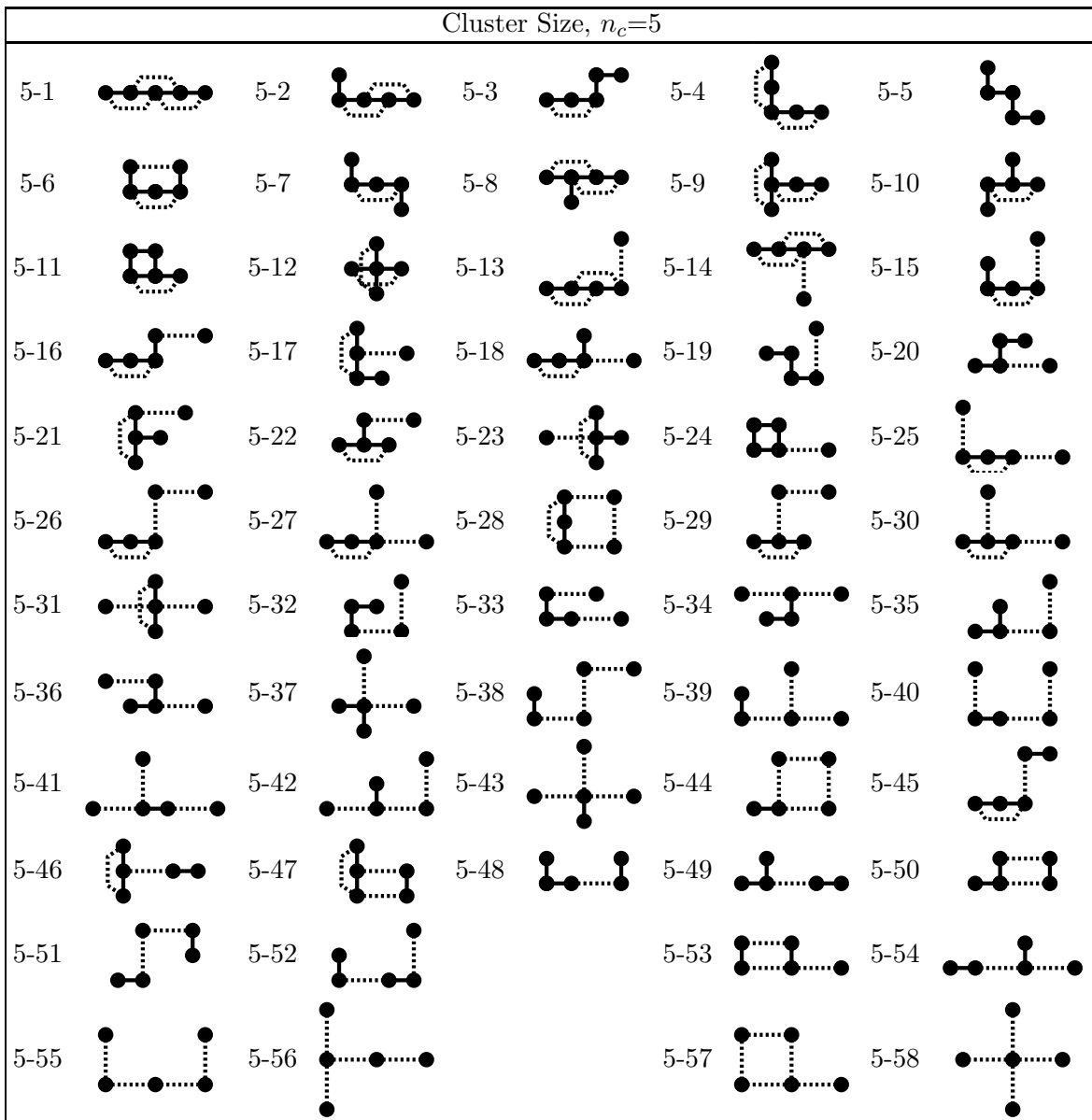


FIG. 4: Cluster types of quintets ( $n_c=5$ ) in the  $J_1$ - $J_3$  model.

nite number of cluster types  $c$ . Usually they are known only for cluster types whose sizes  $n_c$  are no larger than some maximum size  $n_{\max}$ . The sum in Eq.( 2) is therefore truncated after the finite sum over cluster types with  $n_c \leq n_{\max}$  is evaluated exactly. The remainder (REM) from clusters of sizes  $n_c > n_{\max}$ , is then approximated by the “remainder correction”  $R(T, B)$ . In the present work,  $n_{\max}=5$ , so that the REM is from clusters larger than quintets. The remainder correction  $R(T, B)$  was obtained by the corrective quintets (CQUIN’s) method. The application of this method to the NN cluster model was discussed in I. For a model with two exchange constants the CQUIN’s method is considerably more involved.

The number of spins in the REM is  $P_{>5}N_{\text{total}}$ . The accuracy of the CQUIN’s method is not an important issue

if  $P_{>5} \ll 1$ . Because  $P_{>5}$  increases with  $x$ , the accuracy is not a significant issue if  $x$  is sufficiently small. All magnetization curves in the present paper are for  $x \leq 0.09$ , and are based on the  $J_1$ - $J_2$  model. Under these conditions,  $P_{>5} \leq 3.6\%$ , so that errors in  $M$  resulting from the CQUIN’s method are not significant. The description of the CQUIN’s method is postponed to the following paper, which also includes some examples for higher  $x$ .

## B. The two reduced magnetic fields

The two exchange constants,  $J^{(1)}$  and  $J^{(2)}$ , lead to two energy scales for the Zeeman energy. In analogy to Eq. (10) of I, the primary reduced magnetic field  $b_1$  is

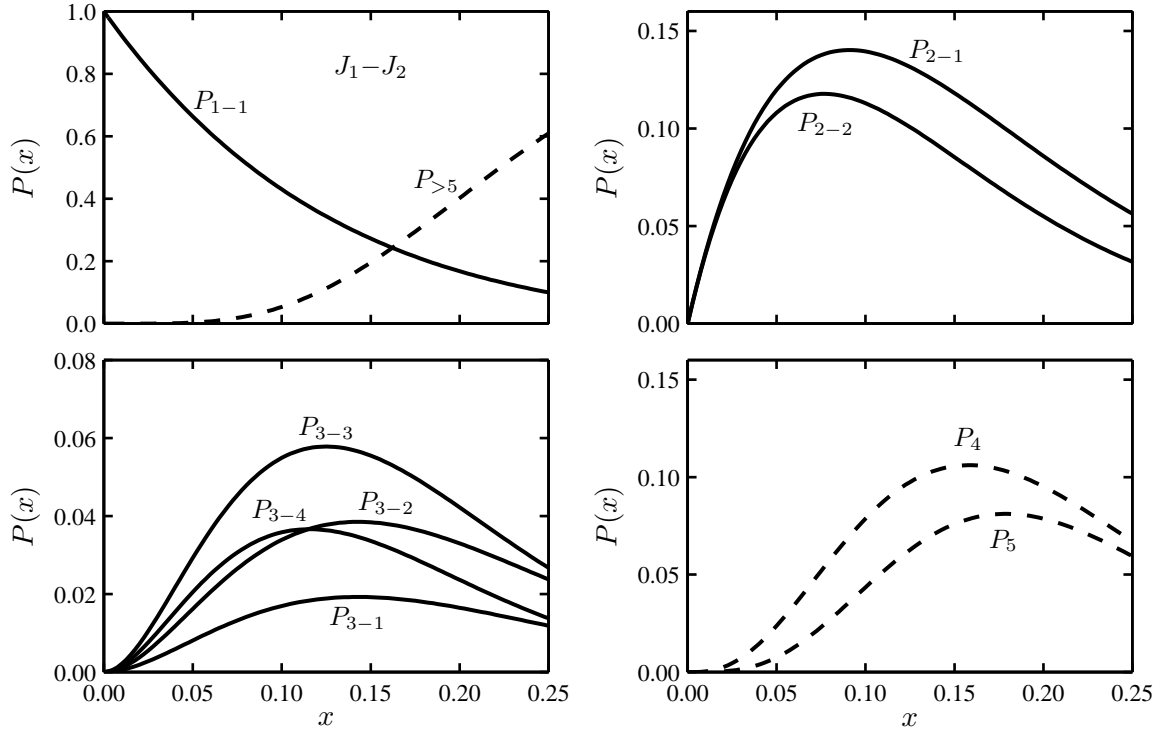


FIG. 5: Probabilities  $P_c$  as a function of  $x$  for some cluster types of the  $J_1$ - $J_2$  model. The solid curves are for individual cluster types, labeled as in Fig. 1. Curve 1-1 is for singles, curves 2-1 and 2-2 are for the two types of pairs, and curves 3-1 up to 3-4 are for the four types of triplets. The dashed curves are probabilities for some combinations of cluster types:  $P_4$  is the sum of the  $P_c$ 's for all the 15 quartet types in Fig. 1;  $P_5$  is the sum of the  $P_c$ 's for all 45 quintet types in Fig. 2; and  $P_{>5}$  is the sum of the probabilities for all cluster types of sizes  $n_c > 5$ .

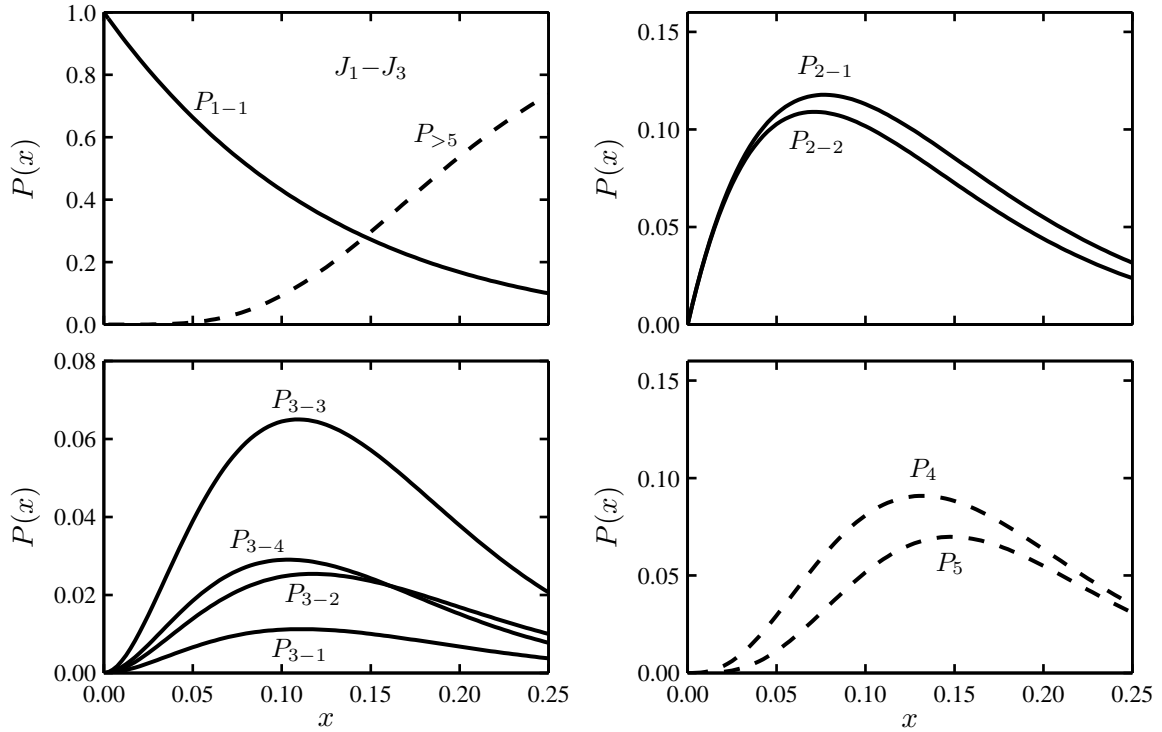


FIG. 6: Probabilities  $P_c$  as a function of  $x$  for some cluster types of the  $J_1$ - $J_3$  model. The labels for the various curves are similar to those in Fig. 5, except that the cluster types refer to Figs. 3 and 4 for the  $J_1$ - $J_3$  model.



defined as

$$b_1 = g\mu_B B / |J^{(1)}|. \quad (3a)$$

The secondary reduced magnetic field  $b_2$  is

$$b_2 = g\mu_B B / |J^{(2)}|. \quad (3b)$$

Thus, at any given  $B$ ,

$$b_1/b_2 = |J^{(2)}/J^{(1)}| < 1. \quad (4)$$

The reduced magnetization  $m$  is defined as in I. That is,

$$m = M/M_0, \quad (5)$$

where  $M_0$  is the true saturation value of  $M$ . The reduced parameters  $b_1$ ,  $b_2$ , and  $m$ , will be used in plots and discussions of the magnetization curves.

### C. MST's from the two different types of pairs

At a low  $T$  the calculated magnetization curve,  $M$  versus  $B$ , includes a superposition of many series of MST's. Each series arises from some cluster type  $c$  of size  $2 \leq n_c \leq n_{\max}$ . The magnitude  $(\Delta M)_c$  of a magnetization jump at each MST in the series is proportional to the population  $N_c$  of the relevant cluster type. For low  $x$  the largest jumps  $(\Delta M)_c$  are for  $J^{(1)}$  pairs and  $J^{(2)}$  pairs. In both  $J_1$ - $J_2$  and  $J_1$ - $J_3$  models these pairs are cluster types 2-1 and 2-2, respectively (see Figs. 1 and 3).

The MST's from  $J^{(1)}$  pairs occur at the primary reduced fields

$$b_1 = 2, 4, 6, \dots, 4S. \quad (6a)$$

The MST's from  $J^{(2)}$  pairs occur when the secondary reduced field has the same values, i.e., at

$$b_2 = 2, 4, 6, \dots, 4S. \quad (6b)$$

Experimental values of the magnetic fields  $B$  at the MST's from pairs are often used to determine  $J^{(1)}$  and  $J^{(2)}$ . The temperature requirement for resolving the MST's from  $J^{(2)}$  pairs is  $k_B T < |J^{(2)}|$ . This is a more stringent requirement than  $k_B T < |J^{(1)}|$  for resolving the MST's from  $J^{(1)}$  pairs.

Equations (6a) and (6b) use the reduced fields  $b_1$  and  $b_2$ . Using the magnetic field  $B$ , instead of the reduced fields, the ranges of  $B$  for the MST series from the two types of pairs may or may not overlap. The condition for avoiding overlap is

$$J^{(2)}/J^{(1)} < 1/2S. \quad (7)$$

For magnetic ions with  $S=5/2$  (e.g.,  $\text{Mn}^{2+}$  or  $\text{Fe}^{3+}$ ) overlap is avoided if  $J^{(2)}/J^{(1)} < 0.2$ .

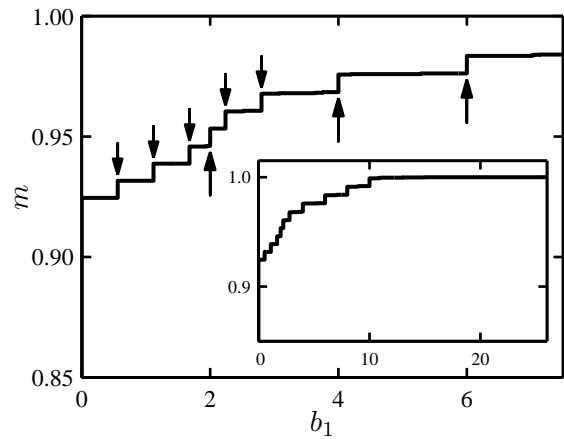


FIG. 7: Magnetization curve at  $T=0$ , calculated from the  $J_1$ - $J_2$  model using the parameters  $x=0.01$ ,  $S=5/2$ , and  $J_2/J_1=0.28$ . The ordinate is the reduced magnetization,  $m=M/M_0$ , where  $M_0$  is the true saturation magnetization. The abscissa is the primary reduced magnetic field  $b_1=g\mu_B B/|J_1|$ , up to 7.5. MST's from  $J_1$  pairs (cluster type 2-1) are indicated by long upward arrows. MST's from  $J_2$  pairs (cluster type 2-2) are indicated by shorter downward arrows. The inset shows the full magnetization curve, up to complete saturation.

### D. Two examples of magnetization curves for very low $x$

The main purpose of the following two examples is to illustrate the dependence of the MST pattern on the ratio  $J^{(2)}/J^{(1)}$ . The examples are for  $x=0.01$  in the  $J_1$ - $J_2$  cluster model. To optimize the resolution of the spectra, the examples are for  $T=0$ . The value  $S=5/2$  is assumed.

Figures 7 and 8 are for  $J_2/J_1=0.28$ . Figure 7 shows the reduced magnetization  $m$  as a function of the primary reduced magnetic field  $b_1$ . MST's from  $J_1$  pairs (cluster type 2-1) are indicated by long arrows, and those from  $J_2$  pairs (cluster type 2-2) by shorter arrows. The main part of Fig. 7 shows the magnetization curve up to  $b_1 = 7.5$ . The full magnetization curve is shown in the inset.

Figure 8 shows the derivative  $dM/dB$ , in normalized units,<sup>11</sup> in fields up to  $b_1 = 7$ , corresponding to the main part of Fig. 7. The upper abscissa scale is for the secondary reduced magnetic field  $b_2$ . The derivative peaks at MST's from  $J_1$ -pairs (type 2-1) and from  $J_2$ -pairs (type 2-2), are indicated by long and short arrows, respectively. Their reduced magnetic fields are given by Eqs. (6a) and (6b). Because the ratio  $J_2/J_1=0.28$  is higher than 0.2, the field ranges for the series of MST's from the two types of pairs overlap.

Figure 9 shows the magnetization (top) and derivative (bottom) curves for  $x=0.01$  when the ratio  $J_2/J_1=0.028$ , i.e., smaller by a factor of 10 compared to the ratio in Figs. 7 and 8. All other parameters are the same as for Figs. 7 and 8. Because the ratio  $J_2/J_1$  is now well below 0.2, the MST series from  $J_1$ - and  $J_2$ -pairs occur in field ranges that do not overlap. In the "gap" between

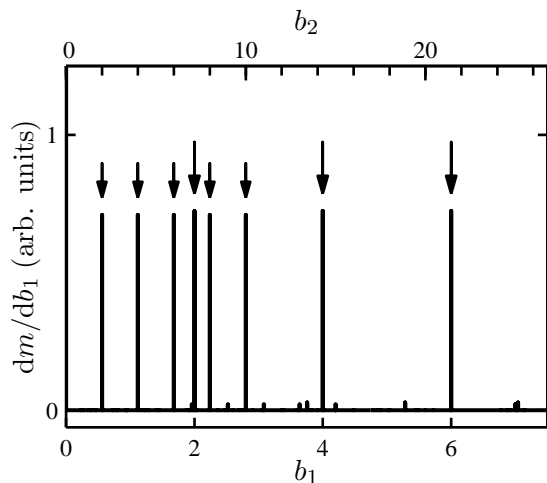


FIG. 8: The derivative of the magnetization curve in Fig. 7. The ordinate is the derivative  $dm/db_1 = (|J_1|/g\mu_B M_0)(dM/dB)$ . The lower abscissa scale is for the primary reduced field  $b_1$ . The upper abscissa scale is for the secondary reduced magnetic field  $b_2$ . The derivative peaks at MST's from cluster types 2-1 ( $J_1$  pairs) and 2-2 ( $J_2$  pairs) are indicated by long and short arrows, respectively.

these two field ranges, the magnetization (upper curve) exhibits a plateau of apparent saturation, labeled as  $m_s$ . The apparent saturation value,  $m_s=0.961$ , agrees with the value of  $m_s$  obtained from the NN cluster model for this  $x$  (Ref.1). However, in contrast to the NN cluster model, the apparent saturation is reached only after the series of MST's from the  $J_2$  pairs (type 2-2) is completed. Clearly, the MST pattern for  $J_2/J_1=0.028$  (Fig. 9) is much simpler than that for  $J_2/J_1=0.28$  (Figs. 7 and 8).

Figure 7 for  $J_2/J_1=0.28$  shows a short magnetization plateau immediately after the initial magnetization rise. This plateau, which ends at the first MST from  $J_2$  pairs (not  $J_1$  pairs), is not the plateau of apparent saturation predicted by the NN cluster model. The value  $m=0.925$  at the first short plateau in Fig. 7 is well below the apparent saturation value  $m_s=0.961$  in the NN cluster model. The reason for the lower value is that the series of MST's from  $J_2$  pairs has not been completed before the start of this short plateau.

## VI. THE MST SPECTRUM

### A. Spectrum

The derivative  $dM/dB$  as a function of  $B$  exhibits a peak at each MST. The pattern of the peaks in the derivative curve will be called the ‘‘MST spectrum.’’ Figure 8 and the lower curve in Fig. 9 are examples of such MST spectra. Each peak in  $dM/dB$  is a ‘‘spectral line.’’ Two or more spectral lines associated with MST's arising from different cluster types may overlap. When a spectral line

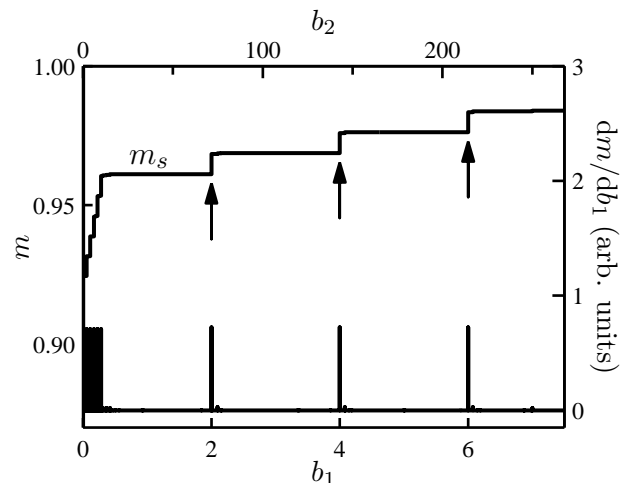


FIG. 9: Zero-temperature magnetization curve (upper curve) and its derivative (lower curve) for  $x=0.01$ . These curves are calculated using the  $J_1$ - $J_2$  model and the ratio  $J_2/J_1=0.028$ . As in Fig. 8 the lower and upper abscissa scales are for  $b_1$  and  $b_2$ , respectively. The left ordinate scale is for  $m$ . The right ordinate scale is for  $dm/db_1$ . The arrows indicate the locations of the MST's from  $J_1$  pairs (type 2-1). The MST's from  $J_2$  pairs (type 2-2) are bunched up at low fields. The plateau of apparent saturation is labeled as  $m_s$ .

is due to only one MST from one cluster type  $c$ , the integral of the spectral line with respect to  $B$  is equal to the magnetization jump  $(\Delta M)_c$ .

There are several advantages of using the spectrum. A plot of the spectrum,  $dM/dB$  versus  $B$ , is very effective in conveying information visually. Another advantage is that the calculated spectrum is the *exact* spectrum from cluster types with  $n_c \leq n_{\max}$ .

As discussed earlier, the infinite sum in Eq. (2) is split into a sum over clusters with  $n_c \leq n_{\max}$ , and a remainder (REM) from larger clusters ( $n_c > 5$  in the present work). The reason for the split is that the Hamiltonians of clusters with  $n_c > n_{\max}$  have not been diagonalized. The finite sum is evaluated exactly, but the REM is approximated by  $R(T, B)$ . The derivative of  $R(T, B)$  does not give the spectral lines from the clusters with  $n_c > n_{\max}$ . These lines can be obtained only if cluster Hamiltonians for  $n_c > n_{\max}$  are diagonalized.

A wealth of information, such as accurate exchange constants, can be obtained from a comparison of an experimental spectrum with the calculated exact spectrum for  $n_c \leq n_{\max}$ . All the spectra shown in this paper are the derivatives of the exact finite sum up to  $n_{\max}=5$ , without the remainder (see Ref. 12).

### B. Additional examples of MST patterns and spectra

The examples in Sec. VD, for  $J_2/J_1=0.28$  and  $0.028$ , assumed  $x=0.01$ . The following examples are for the

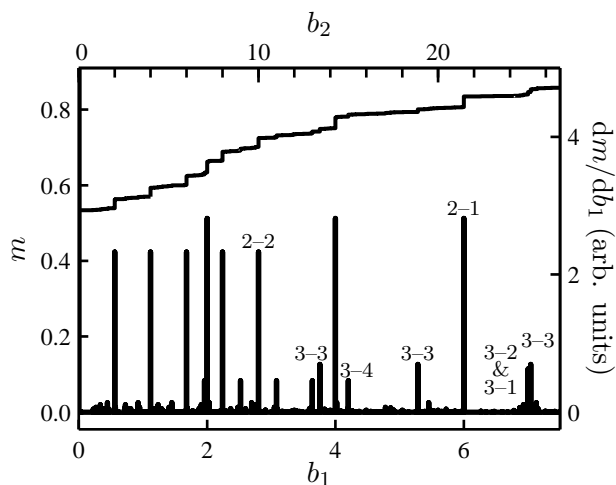


FIG. 10: The reduced magnetization  $m$  (top curve) and the MST spectrum (lower curve) at  $T=0$  for  $x=0.09$ ,  $S=5/2$ . These curves are for  $J_2/J_1=0.28$ . Only the results in the range  $b_1 < 7.5$  are shown. The cluster types responsible for some of the spectral lines are indicated.

same ratios  $J_2/J_1$ , but for higher  $x$ . All other parameters ( $S=5/2$ ,  $T=0$ ), and the cluster model ( $J_1$ - $J_2$ ), are the same as in Sec. VD. An example of a zero-temperature spectrum calculated from the  $J_1$ - $J_3$  model will be given in the following paper.<sup>7</sup> Calculated spectra at finite temperatures will be shown in Ref. 13 in connection with analysis of experimental data.

### 1. Magnetization curves and spectra for $x=0.09$

Magnetization curves and spectra for  $x=0.09$  are shown in Figs. 10 and 11. From Fig. 5 the probabilities  $P_c$  for all four triplet types increase when  $x$  changes from 0.01 to 0.09. The largest increase is for triplet type 3-3, which is a  $J_1$  pair attached to a third spin by a  $J_2$  bond. As a result, spectral lines from type 3-3 triplets are readily seen in Figs. 10 and 11.

Figure 10 shows the MST pattern (top curve) and the MST spectrum (lower curve) for  $x=0.09$  when  $J_2/J_1=0.28$ . The range of the primary reduced field is  $b_1 < 7.5$ . The cluster types responsible for some prominent spectral lines are indicated. Clearly, for  $J_2/J_1 = 0.28$  the spectrum is quite complicated because of the overlap between different series of MST's from different cluster types.

Figure 11 shows the results for the same  $x$  when  $J_2/J_1=0.028$ . For this much lower  $J_2/J_1$  ratio, the spectrum is much simpler. All the discernable spectral lines occur in two separate field ranges. The top of the low-field range is slightly above  $b_1=0.42$  where the series from type 3-4 triplets ends. The bottom of the high-field range is near  $b_1=0.935$  where a small MST from quartet type 4-2 is barely discernable. The two field ranges are separated by a gap, i.e., by a field range in which there are

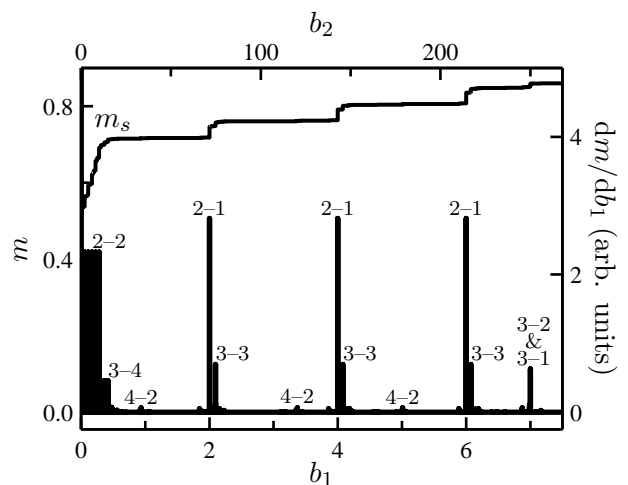


FIG. 11: Zero-temperature magnetization curve (top curve) and spectrum (lower curve) for  $x=0.09$ , calculated from the  $J_1$ - $J_2$  model when  $J_2/J_1=0.028$ . The range of the primary reduced field is limited to  $b_1 < 7.5$ . The plateau of apparent saturation is labeled as  $m_s$ .

no discernable spectral lines. The absence of discernable lines implies that  $m$  has reached a plateau. The value  $m=0.715$  at this plateau agrees with the apparent saturation value  $m_s$  calculated from the NN cluster model.

In the field range of Fig. 11 the  $J_1$  pairs, which exist both in the  $J_1$  and the  $J_1$ - $J_2$  models, give rise to large MST's at  $b_1=2, 4, 6$ . These are the 2-1 lines in Fig. 11. Near each 2-1 line there is also a line from the 3-3 triplets. The 3-3 lines do not exist in the  $J_1$  model. Each 3-3 line together with the stronger nearby 2-1 line may be viewed as a fine structure (FS) that has evolved from a single spectral line, due to  $J_1$  pairs, in the  $J_1$  model. The separation  $\Delta b_2$ , in the secondary reduced field, between the 3-3 line and the nearby 2-1 line is of order 1. The corresponding magnetic field separation  $\Delta B$  is  $g\mu_B\Delta B \sim |J_2|$ .

Figure 11 also shows a spectral line at  $b_1=7$  labeled as 3-2 & 3-1. It corresponds to the coincidence of the first MST from triplets of type 3-1 and the first MST from triplets of type 3-2. The ‘‘intensity’’ of this combined line is just the sum of the two intensities. The other lines from the 3-1 and 3-2 triplets, at  $b_1=9, 11, 13$  and 15 (above the field range of Fig. 11), also coincide when  $J_2/J_1=0.028$ . Figure 10 shows that the 3-1 and 3-2 lines still coincide when  $J_2/J_1=0.28$ . It can be shown that this remains true as long as  $J_2/J_1 \leq 1$ . For additional details see Ref. 14.

### 2. Spectrum for $x=0.20$

For  $x=0.20$ , approximately 40% of the spins are in clusters of sizes  $n_c \geq 5$  (see Fig. 5). When such a large fraction of the spins are in the REM of Eq. (2), the accuracy of the CQUIN's method of treating the magnetization from the REM is open to question. Under these circumstances,

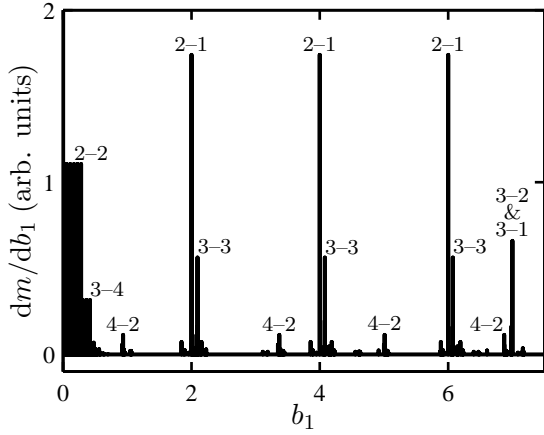


FIG. 12: Zero-temperature spectrum in the  $J_1$ - $J_2$  model for  $J_2/J_1=0.028$  when  $x=0.20$ . Cluster types responsible for some spectral lines are indicated.

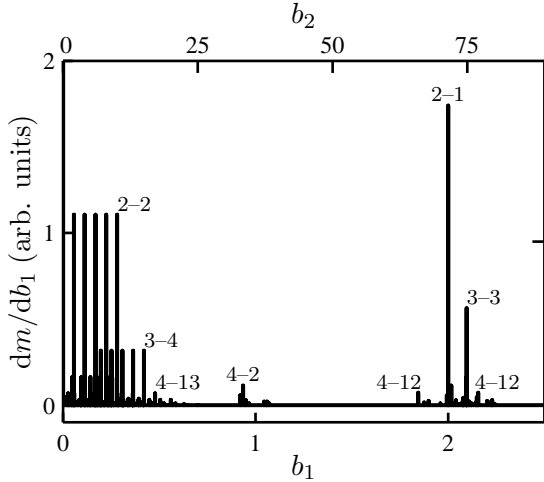


FIG. 13: Expanded view of the spectrum in Fig. 12 ( $x=0.20$ ) for the range  $0 < b_1 < 2.5$ .

a plot of the exact spectrum for clusters with  $n_c \leq 5$  is probably preferable to a plot of the magnetization curve.

The calculated spectrum for  $x=0.20$  will be shown only for the low ratio  $J_2/J_1=0.028$ . Figure 12 shows this spectrum in the range  $0 < b_1 < 7.5$ , at  $T=0$ . Cluster types responsible for some of the spectral lines are indicated. An expanded view of the spectrum in the range  $b_1 < 2.5$  is shown in Fig. 13. The comparison of Figs. 12 and 13 with Fig. 11 shows that the increase of  $x$  from 0.09 to 0.20 has led to the following changes:

1. There are new discernable lines. Some of these new lines are in the FS near  $b_1=2$ . Two of the lines in this FS are from cluster type 4-12. One of these 4-12 lines is slightly above the 2-1 line (from pure  $J_1$  pairs in the  $J_1$ - $J_2$  model), and the other 4-12 line is slightly below it. Actually there is even a stronger new line in the same FS from quartets of type 4-10. However, this line is not resolved be-

cause it is very close to the still stronger line from the 3-3 triplets.

2. A gap, in which there are no discernable spectral lines, separates the low-field and high-field parts of the spectrum. On the scale of Fig. 13 there are no discernable lines between  $b_1=0.63$  and  $b_1=0.92$ .

## VII. LOPSIDED MODELS

The spectra for a “very small” ratio  $J_2/J_1$ , are shown in Figs. 9, and 11–13. These spectra are relatively simple. They suggest<sup>15</sup> the following five features for such small  $J_2/J_1$  ratios.

1. The spectrum consists of a low-field part and a high-field part, separated by a gap in which there are no discernable spectral lines.
2. In the field range of the gap, the magnetization exhibits apparent saturation, with an apparent saturation value  $m_s$  equal to that given by the NN cluster model.
3. In the high-field part of the spectrum, many spectral lines that exist in the parent  $J_1$  model develop a FS. The most conspicuous FS evolves from those lines in the  $J_1$  model that are due to  $J_1$ -pairs, i.e., the lines at  $b_1=2, 4, 6$ , etc.
4. Separations between adjacent lines in the FS that has evolved from a single line in the  $J_1$  model are of order  $\Delta b_2 \sim 1$ . The corresponding separations  $\Delta B$  are of order  $g\mu_B B \Delta B \sim |J_2|$ .
5. In the low-field part of the spectrum, the separations between adjacent lines are also of order  $\Delta b_2 \sim 1$ , or  $g\mu_B B \Delta B \sim |J_2|$ .

The same five features are also found in simulations that use the  $J_1$ - $J_3$  model when the ratio  $J_3/J_1$  is “very small.”

When the ratio  $J^{(2)}/J^{(1)}$  is sufficiently small that the five features listed above appear in the spectrum, the  $J^{(2)}$ - $J^{(1)}$  model is called “lopsided.” Spectra from lopsided models are discussed in detail in the following paper. Far from a mere curiosity, lopsided models actually apply to many materials. In Ref. 13, which appears in this issue, the theoretical results for lopsided models will be used to interpret data obtained in  $(C_3NH_3)_2Mn_xCd_{1-x}Cl_4$  near 20 mK.

## Acknowledgments

This work was supported by CNPQ and FAPESP. Travel funds for Y. S. were also provided by FAPESP.

## APPENDIX A: ISOMORPHISM OF THE PARENT $J_1$ , $J_2$ , AND $J_3$ MODELS

Starting from Fig. 1 of I, and using symmetry arguments<sup>16</sup> one can show that the cluster types of the

$J_1$ -model, of the  $J_2$ -model, and of the  $J_3$ -model, are identical except for the difference in the symmetry class of the neighbor associated with the (only one) exchange constant  $J$  that is included in the model. That is, the bond lists for all cluster types in the  $J_2$  model can be obtained from those in the  $J_1$  model by replacing the label 1 for NN's by the label 2 for 2nd neighbors. The bond lists in the  $J_3$  model are also the same, except that the label 3 for the 3rd neighbors replaces the label 1. Different cluster models, each with only one exchange constant, whose bond lists are related in this manner will be called "isomorphic." Corresponding cluster types in isomorphic cluster models will be called isomorphic cluster types.

The exchange part of the cluster Hamiltonian is specified by the bond list for that cluster type.<sup>1</sup> Cluster Hamiltonians of isomorphic cluster types are identical except for the numerical value of the only  $J$  (see Ref. 17). Each cluster type, except the single, leads to a series of MST's. The magnetic fields at the MST's originating from isomorphic cluster types are the same except for a scale factor which is proportional to the  $J$  in the model.

For the three parent cluster models considered here, the probabilities  $P_c$  for isomorphic cluster types are the same. The site percolation concentrations for these three models are also the same.<sup>9</sup> It is noteworthy that for the square lattice the  $J_4$ -model is not isomorphic to the  $J_1$ ,  $J_2$ , and  $J_3$  models. This difference can be understood from Fig. 1 of I. The number of 4th neighbors surrounding the central cation site is 8, compared to 4 for the 1st, 2nd, and 3rd neighbors.

#### APPENDIX B: BOND LISTS AND PERIMETER POLYNOMIALS FOR THE $J_1$ - $J_2$ AND THE $J_1$ - $J_3$ CLUSTER MODELS

Tables I and II in give the bond lists, and the perimeter Polynomials,  $D_c(q)$ , for the cluster types of the  $J_1$ - $J_2$  model. The cluster types  $c$ , limited to sizes  $n_c \leq 5$ , are those shown in Figs. 1 and 2.

Tables III and IV in this Appendix give the bond lists, and the perimeter Polynomials,  $D_c(q)$ , for the cluster types of the  $J_1$ - $J_3$  model. The cluster types  $c$  are those shown in Figs. 3 and 4.

#### APPENDIX C: RELATIONS BETWEEN "PURE" CLUSTER TYPES AND CLUSTER TYPES IN THE PARENT MODELS

Consider first the cluster types of the  $J_1$ - $J_2$  model (Figs. 1 and 2). At the bottom of these figures are the "single" (type 1-1) and the nine pure  $J_2$  cluster types. Together, they are identical to the 10 cluster types of the (parent)  $J_2$  model. As pointed out in Appendix A the cluster types of the  $J_2$  model are isomorphic to the cluster types of the  $J_1$  model. The pictorial representations of the cluster types of the  $J_1$  model, shown earlier

Cluster type, $c$	Bond List	$D_c(q)$
1-1	{}	$q^8$
2-1	{1}	$2q^{10}$
2-2	{2}	$2q^{12}$
3-1	{11;0}	$2q^{12}$
3-2	{11;2}	$4q^{12}$
3-3	{12;0}	$8q^{14}$
3-4	{22;0}	$4q^{15}+2q^{16}$
4-1	{110;01;0}	$2q^{14}$
4-2	{121;10;0}	$8q^{14}$
4-3	{112;21;0}	$4q^{14}$
4-4	{111;22;0}	$4q^{14}$
4-5	{211;11;2}	$q^{12}$
4-6	{110;02;0}	$8q^{16}$
4-7	{110;22;0}	$8q^{15}+8q^{16}$
4-8	{112;20;0}	$4q^{16}$
4-9	{120;02;0}	$8q^{18}$
4-10	{120;00;2}	$16q^{17}+8q^{18}$
4-11	{122;00;0}	$4q^{17}$
4-12	{210;01;0}	$8q^{16}$
4-13	{220;02;0}	$4q^{18}+8q^{19}+2q^{20}$
4-14	{222;00;0}	$4q^{18}$
4-15	{022;22;0}	$q^{17}$

TABLE I: Bond lists and perimeter polynomials  $D_c(q)$  for cluster types of sizes  $1 \leq n_c \leq 4$  in the  $J_1$ - $J_2$  model. The labels for the cluster types are as in Fig. 1.

in Fig. 3 of I, are therefore also applicable to the cluster types of the  $J_2$  model.

There are only four pure  $J_1$  cluster types in the  $J_1$ - $J_2$  model. Together with the single, they comprise only a subset of the 10 cluster types of the parent  $J_1$  model (Fig. 3 of I). The reason why some cluster types of the  $J_1$  model are not among the pure  $J_1$  cluster types of the  $J_1$ - $J_2$  model is the following. As discussed in Sec. II A 3, all cluster configurations that are present in the  $J_1$  model are also present in the  $J_1$ - $J_2$  model. Some of these configurations have two  $J_1$  bonds that are: 1) connected to the same spin, and 2) make a  $90^\circ$  angle with each other. In the  $J_1$ - $J_2$  model, each such configuration has at least one  $J_2$  bond, so that it is a configuration of a mixed cluster of the  $J_1$ - $J_2$  model, not a configuration of a pure  $J_1$  cluster. If all configurations of a particular cluster type  $c$  of the  $J_1$  model contain consecutive  $J_1$  bonds that make a  $90^\circ$  angle, then this cluster type is not among the pure  $J_1$  cluster types of the  $J_1$ - $J_2$  model.

Two  $J_1$  bonds that are connected to the same spin are either at a  $90^\circ$  angle or at a  $180^\circ$  angle with each other. Consider the pure  $J_1$  cluster types that exist in the  $J_1$ - $J_2$  model. Each such cluster type has only one configuration in this model. All the spins in this configuration are on a single straight line. In the parent  $J_1$  model, on the other

Cluster type, $c$	Bond List	$D_c(q)$	$c$	Bond List	$D_c(q)$
5-1	{0110;101;00;0}	$2q^{16}$	5-23	{1100;020;00;2}	$16q^{19}+8q^{20}$
5-2	{1120;010;01;0}	$8q^{16}$	5-24	{1100;220;02;0}	$8q^{19}+4q^{20}$
5-3	{1210;120;01;0}	$8q^{16}$	5-25	{1100;222;00;0}	$8q^{18}$
5-4	{2110;101;00;0}	$4q^{16}$	5-26	{1100;220;00;2}	$8q^{18}+24q^{19}+8q^{20}$
5-5	{1122;210;01;0}	$4q^{16}$	5-27	{1100;220;02;2}	$4q^{17}$
5-6	{1122;010;01;0}	$4q^{15}+4q^{16}$	5-28	{1120;202;00;0}	$8q^{19}+8q^{20}$
5-7	{1110;201;20;0}	$8q^{16}$	5-29	{1120;200;00;2}	$8q^{19}+4q^{20}$
5-8	{1110;221;00;0}	$4q^{16}$	5-30	{1022;200;00;0}	$8q^{21}$
5-9	{1112;201;20;0}	$8q^{16}$	5-31	{1200;002;20;0}	$8q^{20}+24q^{21}+16q^{22}$
5-10	{1121;212;10;0}	$8q^{14}$	5-32	{1200;000;20;2}	$16q^{20}+32q^{21}+8q^{22}$
5-11	{1111;022;22;0}	$q^{16}$	5-33	{1200;000;22;0}	$24q^{20}$
5-12	{1100;010;02;0}	$8q^{18}$	5-34	{1220;000;02;0}	$8q^{20}+8q^{21}$
5-13	{1102;210;00;0}	$8q^{18}$	5-35	{1022;000;22;0}	$4q^{19}$
5-14	{1120;010;02;0}	$16q^{18}$	5-36	{1010;200;01;0}	$16q^{18}$
5-15	{1210;100;02;0}	$8q^{17}+8q^{18}$	5-37	{1100;220;00;1}	$16q^{17}+16q^{18}$
5-16	{1120;210;02;0}	$8q^{17}+8q^{18}$	5-38	{2110;001;20;0}	$8q^{18}$
5-17	{1122;210;00;0}	$8q^{17}$	5-39	{0210;102;00;0}	$32q^{20}$
5-18	{1110;220;02;0}	$8q^{17}+8q^{18}$	5-40	{2102;010;00;0}	$16q^{19}$
5-19	{1110;222;00;0}	$8q^{17}$	5-41	{0102;012;00;0}	$4q^{18}+12q^{19}+8q^{20}$
5-20	{2112;110;20;0}	$4q^{16}$	5-42	{0220;202;00;0}	$4q^{21}+16q^{22}+12q^{23}+2q^{24}$
5-21	{1100;020;02;0}	$8q^{20}$	5-43	{2022;200;00;0}	$8q^{21}+12q^{22}$
5-22	{1100;022;00;0}	$4q^{19}$	5-44	{0222;220;00;0}	$8q^{20}$
			5-45	{2222;000;00;0}	$q^{20}$

TABLE II: Bond lists and perimeter polynomials,  $D_c(q)$ , for the quintet types ( $n_c=5$ ) of the  $J_1$ - $J_2$  model. The labels for the cluster types are as in Fig. 2.

hand, the same pure  $J_1$  cluster type, with the exception of cluster type 2-1, has several configurations. For example, cluster type 3 in Fig. 3 of I has two configurations in the  $J_1$  model (configurations  $3\alpha$  and  $3\beta$  in Fig. 4 of I). The same cluster type exists in the  $J_1$ - $J_2$  model as cluster type 3-1 (Fig. 1 of the present paper), but the only configuration is  $3\alpha$ , with the two  $J_1$  bonds at  $180^\circ$  angle.

Similar results are obtained for the pure cluster types in the  $J_1$ - $J_3$  model: 1) The pure  $J_3$  cluster types of this model, together with the single, are identical to the 10 cluster types of the parent  $J_3$  model. 2) The pure  $J_1$  cluster types, together with the single, are only a subset of the cluster types of the parent  $J_1$  model. In this case, the reason why they are only a subset is that in the  $J_1$ - $J_3$  model any configuration that has two consecutive  $J_1$  bonds at  $180^\circ$  angle, also has at least one  $J_3$  bond. Therefore, in the  $J_1$ - $J_3$  model it is a configuration of a mixed cluster, not of a pure  $J_1$  cluster. If all configurations of a particular cluster type  $c$  of the  $J_1$  model contain consecutive  $J_1$  bonds that make  $180^\circ$  angle, then this cluster type is not among the pure  $J_1$  cluster types of the  $J_1$ - $J_3$  model.

To follow up on the previous example of cluster type 3 in Fig. 3 of I, this cluster type is identical to cluster type 3-2 in the  $J_1$ - $J_3$  model (Fig. 3 of the present paper),

which is a pure- $J_1$  cluster type. Cluster type 3-2 of the  $J_1$ - $J_3$  model has only one configuration, namely, the  $3\beta$  configuration in which the two consecutive  $J_1$  bonds are at  $90^\circ$  angle.

#### APPENDIX D: COMMENTS ON THE PROBABILITIES OF PURE CLUSTER TYPES IN THE $J_1$ - $J_2$ AND $J_1$ - $J_3$ MODELS

As discussed in Appendix C, the pure  $J_2$  cluster types of the  $J_1$ - $J_2$  model are identical to cluster types of the parent  $J_2$  model. The configurations for each of these cluster types are also the same in the two models. However, the probability  $P_c$  for each of these cluster types is lower in the  $J_1$ - $J_2$  model than in the  $J_2$  model. The reason is that the  $J_1$ - $J_2$  perimeter for any configuration is larger than the  $J_2$  perimeter for the same configuration (see Sec. II C). Similar remarks also apply to the probabilities for the pure  $J_3$  cluster types in the  $J_1$ - $J_3$  model, compared to the probabilities for the same cluster types in the parent  $J_3$  model.

The case of the pure  $J_1$  cluster types is somewhat different. Each of the pure  $J_1$  cluster types in the  $J_1$ - $J_2$  model is identical to one of the cluster types in the par-

Cluster type, $c$	Bond List	$D_c(q)$
1-1	{}	$q^8$
2-1	{1}	$2q^{12}$
2-2	{3}	$2q^{13}$
3-1	{11;3}	$2q^{16}$
3-2	{11;0}	$4q^{15}$
3-3	{13;0}	$8q^{16}+4q^{17}$
3-4	{33;0}	$4q^{17}+2q^{18}$
4-1	{113;31;0}	$2q^{20}$
4-2	{131;10;0}	$8q^{18}$
4-3	{110;01;0}	$4q^{18}$
4-4	{111;30;0}	$4q^{18}$
4-5	{011;11;0}	$q^{16}$
4-6	{110;33;0}	$8q^{19}+4q^{21}$
4-7	{113;30;0}	$4q^{19}$
4-8	{110;03;0}	$16q^{19}+8q^{20}$
4-9	{113;00;0}	$8q^{19}$
4-10	{130;03;0}	$4q^{20}+8q^{21}+2q^{22}$
4-11	{130;00;3}	$16q^{20}+16q^{21}+4q^{22}$
4-12	{133;00;0}	$12q^{20}$
4-13	{130;03;1}	$2q^{18}$
4-14	{310;01;0}	$4q^{19}+8q^{20}+2q^{21}$
4-15	{330;03;0}	$4q^{21}+8q^{22}+2q^{23}$
4-16	{333;00;0}	$4q^{21}$
4-17	{033;33;0}	$q^{20}$

TABLE III: Bond lists and perimeter polynomials,  $D_c(q)$ , for cluster types of the  $J_1$ - $J_3$  model that have sizes  $1 \leq n_c \leq 4$ . The labels for the cluster types are as in Fig. 3.

ent  $J_1$  model. However, the probability  $P_c$  is lower in the  $J_1$ - $J_2$  model, for two reasons. One is that, with the exception of cluster type 2-1, the number of configurations in the  $J_1$ - $J_2$  model is smaller than in the parent  $J_1$  model (see Appendix C). The second reason is that for those configurations that exist in both models, the  $J_1$ - $J_2$  perimeter is larger than the  $J_1$  perimeter. A larger perimeter implies a lower probability for the configuration. For the same two reasons the probability  $P_c$  for any pure  $J_1$  cluster types in the  $J_1$ - $J_3$  model is lower than that for the same cluster type in the  $J_1$  model.

\* Electronic address: yshapira@granite.tufts.edu

† Electronic address: vbindilatti@if.usp.br

<sup>1</sup> V. Bindilatti and Y. Shapira, Phys. Rev. B **72**, 064414 (2005), URL <http://link.aps.org/abstract/PRB/v72/e064414>.

<sup>2</sup> Y. Shapira and V. Bindilatti, J. Appl. Phys. **92**, 4155 (2002), URL <http://link.aip.org/link/?jap/92/4155>.

<sup>3</sup> T. Q. Vu, V. Bindilatti, Y. Shapira, E. J. McNiff, Jr., C. C. Agosta, J. Papp, R. Kershaw, K. Dwight, and A. Wold, Phys. Rev. B **46**, 11617 (1992), URL <http://publish.aps.org/abstract/PRB/v46/p11617>.

<sup>4</sup> V. Bindilatti, E. ter Haar, N. F. Oliveira, Jr., Y. Shapira, and M. T. Liu, Phys. Rev. Lett. **80**, 5425 (1998), URL <http://publish.aps.org/abstract/PRL/v80/p5425>.

<sup>5</sup> V. Bindilatti, E. ter Haar, N. F. Oliveira, Jr., Y. Shapira, and M. T. Liu, J. Appl. Phys. **85**, 5950 (1999), URL <http://link.aip.org/link/?jap/85/5950>.

<sup>6</sup> D. Stauffer and A. Aharony, *Introduction to Percolation Theory, Revised* (Taylor & Francis, London, 1994), revised 2nd ed.

<sup>7</sup> Y. Shapira and V. Bindilatti, arXiv:cond-mat/0609715 (2006), <http://arxiv.org/abs/cond-mat/0609715>.

<sup>8</sup> A “realization” of a cluster type is any one cluster of this

type. Similarly, a realization of a configuration is any one set of cation sites arranged in this configuration.

<sup>9</sup> K. Malarz and S. Galam, Phys. Rev. E **71**, 016125 (2005), URL <http://link.aps.org/abstract/PRE/v71/e016125>.

In addition to percolation concentrations, this work also discusses some symmetry properties of neighbors on the square lattice.

<sup>10</sup> H. P. Peters, D. Stauffer, H. P. Holters, and K. Loewenich, Z. Physik B - Condensed Matter **34** (1979).

<sup>11</sup> To avoid infinite values in the derivative,  $dM/dB$  was evaluated at a very low, but non-zero, temperature  $T$ .

<sup>12</sup> Including the derivative of  $R(T, B)$  can lead to an error if  $R(T, B)$  is obtained by the CQUIN’s method. In this method the true clusters with  $n_c > 5$  are replaced by fictitious quintets. Including the derivative of  $R(T, B)$  in the spectrum would lead to an artificial enhancement of spectral lines from quintets.

<sup>13</sup> X. Gratens and *et al.*, to be published (2006).

<sup>14</sup> In the range  $J_2/J_1 \leq 1$  the positions of the five spectral lines from the 3-1 triplets remain exactly at  $b_1 = 7, 9, 11, 13$  and 15. In the same range of  $J_2/J_1$  the 3-2 triplets produce lines at exactly the same fields, so that all the 3-1 lines coincide with 3-2 lines. However, when  $\frac{1}{2} \leq J_2/J_1 \leq 1$ , the

Cluster Type, $c$	Bond List	$D_c(q)$	$c$	Bond List	$D_c(q)$
5-1	{1133;310;01;0}	$2q^{24}$	5-30	{1130;303;00;0}	$8q^{22}+8q^{24}$
5-2	{1310;130;01;0}	$8q^{22}$	5-31	{1133;300;00;0}	$2q^{22}$
5-3	{1130;010;01;0}	$8q^{21}$	5-32	{1100;030;00;3}	$8q^{22}+24q^{23}+32q^{24}+8q^{25}$
5-4	{1133;010;01;0}	$4q^{20}$	5-33	{1100;030;03;0}	$4q^{22}+20q^{23}+8q^{24}+4q^{25}$
5-5	{0110;101;00;0}	$4q^{20}$	5-34	{1100;033;00;0}	$24q^{23}$
5-6	{3110;101;00;3}	$4q^{20}$	5-35	{1130;000;00;3}	$16q^{23}+8q^{24}$
5-7	{3110;101;00;0}	$4q^{20}$	5-36	{1130;003;00;0}	$24q^{23}+16q^{24}$
5-8	{1131;310;00;0}	$8q^{21}$	5-37	{1133;000;00;0}	$4q^{22}$
5-9	{1311;100;00;3}	$4q^{20}$	5-38	{1300;000;30;3}	$16q^{24}+40q^{25}+24q^{26}+4q^{27}$
5-10	{1110;301;00;0}	$8q^{20}$	5-39	{1300;000;33;0}	$24q^{24}+12q^{25}$
5-11	{1101;013;10;0}	$8q^{19}$	5-40	{1300;003;30;0}	$32q^{24}+24q^{25}+24q^{26}+4q^{27}$
5-12	{1111;300;00;3}	$q^{20}$	5-41	{1033;300;00;0}	$8q^{24}+12q^{25}$
5-13	{1130;310;03;0}	$8q^{23}+4q^{25}$	5-42	{1330;000;03;0}	$32q^{24}+24q^{25}$
5-14	{1133;310;00;0}	$8q^{22}$	5-43	{1333;000;00;0}	$4q^{23}$
5-15	{1310;100;03;0}	$16q^{21}+8q^{23}$	5-44	{1033;000;33;0}	$8q^{23}$
5-16	{1130;010;03;0}	$8q^{22}+8q^{23}$	5-45	{1100;330;00;1}	$8q^{22}+8q^{23}+8q^{24}+4q^{25}$
5-17	{1103;310;00;0}	$16q^{21}$	5-46	{3110;001;30;0}	$4q^{23}$
5-18	{1313;100;00;0}	$8q^{21}+8q^{22}$	5-47	{1130;303;00;1}	$8q^{21}$
5-19	{1100;010;03;0}	$8q^{21}+8q^{22}+8q^{23}$	5-48	{1010;300;01;0}	$8q^{21}+24q^{22}+16q^{23}+8q^{24}$
5-20	{1103;010;00;0}	$16q^{22}$	5-49	{3011;100;00;0}	$8q^{22}+8q^{23}$
5-21	{1110;303;00;0}	$16q^{21}+8q^{23}$	5-50	{1301;030;10;0}	$8q^{21}$
5-22	{1110;003;30;0}	$8q^{22}+4q^{23}$	5-51	{0103;013;00;0}	$4q^{22}+20q^{23}+16q^{24}+12q^{25}+2q^{26}$
5-23	{1113;300;00;0}	$4q^{21}$	5-52	{0310;103;00;0}	$8q^{23}+32q^{24}+24q^{25}+4q^{26}$
5-24	{0113;110;00;0}	$8q^{20}$	5-53	{1303;030;10;0}	$16q^{22}$
5-25	{1100;330;03;0}	$4q^{22}+8q^{24}+2q^{26}$	5-54	{3103;010;00;0}	$32q^{23}+24q^{24}$
5-26	{1100;330;00;3}	$8q^{23}+8q^{24}+8q^{25}+4q^{26}$	5-55	{0330;303;00;0}	$4q^{25}+16q^{26}+12q^{27}+2q^{28}$
5-27	{1100;333;00;0}	$4q^{22}+8q^{23}$	5-56	{3033;300;00;0}	$8q^{25}+12q^{26}$
5-28	{1100;330;03;3}	$4q^{22}$	5-57	{0333;330;00;0}	$8q^{24}$
5-29	{1130;300;00;3}	$8q^{23}+4q^{24}$	5-58	{3333;000;00;0}	$q^{24}$

TABLE IV: Bond lists and perimeter polynomials,  $D_c(q)$ , for quintet types ( $n_c=5$ ) of the  $J_1$ - $J_3$  model. The labels for the cluster types are as in Fig. 4.

3-2 triplets produce additional lines at  $b_1 < 7$ . The values of  $b_1$  at these additional lines depend on the ratio  $J_2/J_1$ .

<sup>15</sup> Conclusions based on numerical simulations for specific values of  $S$  and specific ratios  $J_2/J_1$  fall short of being proven. However, the physical arguments in the following paper give strong additional support to these conclusions.

<sup>16</sup> All lattice sites of the square lattice in Fig. 1 of I can be reached from the central site by successive jumps between NN sites. The sublattice consisting of all sites that can be reached from the central site by successive jumps between 2nd neighbors is, by itself, also a square lattice. Compared to the original square lattice, this “new” square lattice has a lattice constant that is a factor of  $\sqrt{2}$  larger, and it is rotated by  $45^\circ$ . The  $J_2$  exchange bonds in the original square lattice are the NN exchange bonds in the new square lattice. All configurations, cluster types, clus-

ter Hamiltonians, and cluster statistics for the original  $J_2$  model are identical to those of the “ $J_1$  model” for the new square lattice. A similar argument applies to the sublattice consisting of all sites that can be reached from the central site by successive jumps between 3rd neighbors.

<sup>17</sup> In a given material the numerical value of  $J$  is specified by the symmetry class of the neighbor associated with  $J$ , i.e., it depends on whether  $J$  is  $J_1$ , or  $J_2$ , or  $J_3$ . However, if the material is not specified then the numerical value of  $J$  is not known even if the symmetry class is known. In that case,  $J$  is just a parameter in the exchange Hamiltonian. As long as it remains just a parameter, there is no difference between the exchange Hamiltonians of isomorphic cluster types.